A Generic Geometrical-Based MIMO Mobile-to-Mobile Channel Model

Xiang Cheng*, Cheng-Xiang Wang*, David I. Laurenson**, Hsiao-Hwa Chen†, and Athanasios V. Vasilakos††
*Joint Research Institute for Signal and Image Processing, Heriot-Watt University, EH14 4AS, Edinburgh, UK.
**Joint Research Institute for Signal and Image Processing, University of Edinburgh, EH9 3JL, Edinburgh, UK.
†Department of Engineering Science, National Cheng Kung University, Taiwan, No.1, University Road, Tainan City 701, Taiwan.
††Department of Computer and Telecommunications Engineering, University of Western Macedonia, GR 50100 Kozani, Greece.
Email: xc48@hw.ac.uk, cheng-xiang.wang@hw.ac.uk, dave.laurenson@ed.ac.uk, hshwchen@ieee.org, vasilako@ath.forthnet.gr

***Abstract*—In this paper, a generic and adaptive geometrical-based stochastic reference model is proposed for multiple-input multiple-output (MIMO) mobile-to-mobile (M2M) Ricean fading channels. The proposed model employs a combined two-ring model and elliptical-ring model, where the received signal is constructed as a sum of the line-of-sight (LoS), single-, and double-bounced rays with different energies. This makes the model sufficiently generic and therefore includes many existing channel models as special cases. Importantly, the model can easily be adapted to a variety of M2M propagation environments, e.g., outdoor macro-, micro, and pico-cells taking into account different vehicle traffic densities, by adjusting model parameters. From the proposed model, the space-time (ST) correlation function (CF) and the corresponding space-Doppler (SD) power spectral density (PSD) of any two sub-channels are derived for a two-dimensional (2D) non-isotropic scattering environment. Finally, some numerical results are presented and compared with measured results. The close agreement between the theoretical and empirical curves verifies the utility of the proposed model.**

I. Introduction

M2M communications play an important role in wireless mobile ad hoc networks, relay-based cellular networks, and intelligent transportation systems, where both the transmitter (Tx) and receiver (Rx) are in motion and equipped with low elevation antennas. For the analysis and design of M2M systems, it is necessary to have a detailed knowledge of the multipath fading channel and its statistical properties. Akki and Haber [1], [2] were the first to propose a channel model for single-input single-output (SISO) M2M Rayleigh fading channels. Their model was extended in [3] to include the line-of-sight (LoS) component resulting in a M2M Ricean fading channel model. In [4], a two-ring model considering only double-bounced rays was presented for MIMO M2M Rayleigh fading channels in outdoor macro-cells. In [5], a more general two-ring model was proposed for MIMO M2M Ricean fading channels in both outdoor macro- and micro-cells by taking into account the LoS, single-bounced, and double-bounced rays. The model in [5] includes the model in [4] as a special case. However, none of the above MIMO M2M channel models [4], [5] is sufficiently general to characterize a wide variety of M2M propagation environments. Especially for pico-cell scenarios, where the distance between the Tx and Rx is relatively small (normally less than 400 m), a combined model consisting of an elliptical ring and two rings seems to be more appropriate. Pico-cell scenarios are currently receiving more and more attention in M2M communications with some measurement campaigns going on [7]. Doppler PSD characteristics for an elliptical-ring MIMO M2M channel model, however, are not known yet.

The objectives are mainly two-fold. First, we aim to propose a generic and adaptive geometrical-based stochastic reference model for ST correlated MIMO M2M Ricean fading channels. Motivated by some interesting observations in [6], we take the impacts of both single- and double-bounced rays into account when proposing this new model. The proposed model employs a combined two-ring model and elliptical-ring model, where the received signal is constructed as a sum of the LoS, single-, and double-bounced rays with different energies. This makes our model sufficiently generic and includes many existing models, e.g., those in [4] and [5], as special cases. More importantly, the model is adaptive to a variety of M2M propagation environments, e.g., outdoor macro-, micro-, and pico-cells taking different vehicle traffic densities into further account, by adjusting model parameters. Second, from the proposed generic model, the ST CF and the corresponding SD PSD are derived for a 2D non-isotropic scattering environment. Closed-form expressions for the above functions are available in the case of the two-ring model with single-bounced rays for the macro- and micro-cell scenarios, and the two-ring model with double-bounced rays for all scenarios. For the two-ring model with single-bounced rays for pico-cell scenarios and the elliptical-ring model for all scenarios, numerical computations for the above functions are necessary while the computation complexity has been reduced with the help of the newly derived relationship between the angle of departure (AoD) and angle of arrival (AoA).

The remainder of this paper is outlined as follows. Section II describes the new adaptive geometrical-based stochastic model for narrowband MIMO M2M Ricean fading channels. In Section III, the ST CF and the corresponding SD PSD are derived. Numerical results and analysis are presented in Section IV. Finally, conclusions are drawn in Section V.

II. An Adaptive Geometrical-based Model

Let us now consider a narrowband single-user MIMO M2M system with M_T transmit and M_R receive omnidirectional

978-1-4244-2202-9/08/$25.00

antenna elements. Both the Tx and Rx are in motion and equipped with antennas mounted at low elevations. The propagation scenario is characterized by non-isotropic scattering with possibly a LoS component between the Tx and Rx.

Fig. 1 illustrates the geometry of the proposed MIMO M2M channel model, which is the combination of a LoS component, a two-ring model with single- and double-bounced rays, and an elliptical-ring model with single-bounced rays. We assume that uniform linear antenna arrays are used with arbitrary numbers of antenna elements. As an example, $M_T = M_R = 2$ were used in Fig. 1. The two-ring model defines two rings of effective scatterers, one around the Tx and the other around the Rx. Suppose there are N_1 effective scatterers around the Tx lying on a ring of radius R_T and the n_1th ($n_1 = 1, ..., N_1$) effective transmit scatterer is denoted by $S_T^{(n_1)}$. Similarly, assume there are N_2 effective scatterers around the Rx lying on a ring of radius R_R and the n_2th ($n_2 = 1, ..., N_2$) effective receive scatterer is denoted by $S_R^{(n_2)}$. The distance between the Tx and Rx is D. For the elliptical-ring model, N_3 effective scatterers lie on an ellipse with the Tx and Rx located at the foci. The semimajor axis of the ellipse and the n_3th ($n_3 = 1, ..., N_3$) effective scatterer are denoted by a and $S_{TR}^{(n_3)}$, respectively. The antenna element spacings at the Tx and Rx are designated by δ_T and δ_R, respectively. It is normally assumed that the radii R_T and R_R and the semimajor axis a are all much larger than the antenna element spacings δ_T and δ_R, i.e., $\min\{R_T, R_R, a\} >> \max\{\delta_T, \delta_R\}$. The multi-element antenna tilt angles are denoted by β_T and β_R. The Tx and Rx move with speeds υ_T and υ_R in directions determined by the angles of motion γ_T and γ_R, respectively. The symbol $\phi_{R_q}^{LoS}$ denotes the AoA of a LoS path. The AoAs of the waves travelling from the effective scatterers $S_T^{(n_1)}$, $S_R^{(n_2)}$, and $S_{TR}^{(n_3)}$ towards the Rx are denoted by $\phi_R^{(n_1)}$, $\phi_R^{(n_2)}$, and $\phi_R^{(n_3)}$, respectively. The AoDs of the waves that impinge on the effective scatterers $S_T^{(n_1)}$, $S_R^{(n_2)}$, and $S_{TR}^{(n_3)}$ are designated by $\phi_T^{(n_1)}$, $\phi_T^{(n_2)}$, and $\phi_T^{(n_3)}$, respectively.

From the above proposed geometrical-based model, the received complex impulse response at the carrier frequency f_c for the $T_p - R_q$ link is a superposition of the LoS, single-, and double-bounced rays can be expressed as

$$h_{pq}(t) = h_{pq}^{LoS}(t) + h_{pq}^{SB}(t) + h_{pq}^{DB}(t) \tag{1}$$

where

$$h_{pq}^{LoS}(t) = \sqrt{\frac{K_{pq}\Omega_{pq}}{K_{pq}+1}} e^{-j2\pi f_c \tau_{pq}} \times e^{j\left[2\pi f_{T_{max}} t \cos\left(\pi - \phi_{R_q}^{LoS} + \gamma_T\right) + 2\pi f_{R_{max}} t \cos\left(\phi_{R_q}^{LoS} - \gamma_R\right)\right]} \tag{2}$$

$$h_{pq}^{SB}(t) = \sum_{i=1}^{I} h_{pq}^{SB_i}(t) = \sum_{i=1}^{I} \sqrt{\frac{\eta_{SB_i}\Omega_{pq}}{K_{pq}+1}} \lim_{N_i \to \infty} \sum_{n_i=1}^{N_i} \frac{1}{\sqrt{N_i}} e^{j\left(\psi_{n_i} - 2\pi f_c \tau_{pq,n_i}\right)} \times e^{j\left[2\pi f_{T_{max}} t \cos\left(\phi_T^{(n_i)} - \gamma_T\right) + 2\pi f_{R_{max}} t \cos\left(\phi_R^{(n_i)} - \gamma_R\right)\right]} \tag{3}$$

$$h_{pq}^{DB}(t) = \sqrt{\frac{\eta_{DB}\Omega_{pq}}{K_{pq}+1}} \lim_{N_1, N_2 \to \infty} \sum_{n_1, n_2 = 1}^{N_1, N_2} \frac{1}{\sqrt{N_1 N_2}} \times e^{j\left(\psi_{n_1,n_2} - 2\pi f_c \tau_{pq,n_1,n_2}\right)} \times e^{j\left[2\pi f_{T_{max}} t \cos\left(\phi_T^{(n_1)} - \gamma_T\right) + 2\pi f_{R_{max}} t \cos\left(\phi_R^{(n_2)} - \gamma_R\right)\right]}. \tag{4}$$

In (2)–(4), $p = 1, 2, ..., M_T$, $q = 1, 2, ..., M_R$, $\tau_{pq} = \epsilon_{pq}/c$, $\tau_{pq,n_i} = (\epsilon_{pn_i} + \epsilon_{n_i q})/c$, $\tau_{pq,n_1,n_2} = (\epsilon_{pn_1} + \epsilon_{n_1 n_2} + \epsilon_{n_2 q})/c$ are the travel times of the waves through the link $T_p - R_q$, $T_p - S_T^{(n_1)}$ ($S_R^{(n_2)}$ or $S_{TR}^{(n_3)}$)$-R_q$, and $T_p - S_T^{(n_1)} - S_R^{(n_2)} - R_q$, respectively. Here, c is the speed of light, $i \in \{1, 2, ..., I\}$, and $I = 3$. The symbol K_{pq} designates the Ricean factor of the $T_p - R_q$ link and Ω_{pq} denotes the total power transferred through the $T_p - R_q$ link. Parameters η_{SB_i} and η_{DB} specify how much the single- and double-bounced rays contribute to the total scattered power $\Omega_{pq}/(K_{pq}+1)$. This indicates that these energy-related parameters satisfy $\sum_{i=1}^{I} \eta_{SB_i} + \eta_{DB} = 1$. The phases ψ_{n_i} and ψ_{n_1,n_2} are independent and identically distributed (i.i.d.) random variables with uniform distributions over $[-\pi, \pi)$, $f_{T_{max}} = \upsilon_T/\lambda$ and $f_{R_{max}} = \upsilon_R/\lambda$ are the maximum Doppler frequencies associated with the Tx and Rx, respectively, and λ is the carrier wavelength.

As mentioned earlier, the proposed model in (1)–(4) is adaptive to a wide variety of M2M propagation environments by adjusting model parameters. It turns out that these important model parameters are the distance D, the energy-related parameters η_{SB_i} and η_{DB}, and the Ricean factor K_{pq}. Based on these parameters the outdoor M2M propagation environments can roughly be categorized into the following four different scenarios: macro-cell, micro-cell, pico-cell with a low vehicle traffic density, and pico-cell with a high vehicle traffic density. For a macro-cell propagation environment, $D \gg \max\{R_T, R_R\}$ holds. The Ricean factor K_{pq} and the energy parameter η_{SB_3} related to the single-bounced elliptical-ring model are very small or even close to zero. The received powers mainly come from the single- and double-bounced rays two-ring model. Based on the investigations in [6], we assume that double-bounced rays bear more energy than single-bounced rays since the AoAs and AoDs are highly independent in such scenarios, i.e., $\eta_{DB} > \max\{\eta_{SB_1}, \eta_{SB_2}\} \gg \eta_{SB_3}$. This means that a macro-cell scenario can be well characterized by using a two-ring model with the negligible LoS component. For a micro-cell propagation environment, the inequality $D \gg \max\{R_T, R_R\}$ is still fulfilled, but the values of K_{pq} and η_{SB_3} in general cannot be neglected unlike a macro-cell scenario. The received power still mainly comes from the single- and double-bounced two-ring models, while the single-bounced rays bear more energy than the double-bounced rays due to the dependence between the AoAs and AoDs, i.e., $\min\{\eta_{SB_1}, \eta_{SB_2}\} > \eta_{DB} > \eta_{SB_3}$. Therefore, a micro-cell scenario is characterized here by using a combined two-ring model and elliptical-ring model, which is more realistic than the two-ring model presented in [5]. For a pico-cell propagation environment, the condition $D \gg \max\{R_T, R_R\}$ is not satisfied anymore, which makes the simplified and widely used relation between the AoD and AoA for the two-ring model

with single-bounced rays unobtainable [5]. This forces us to find a new relation between them. A pico-cell propagation environment can further be classified into the following two scenarios. When there is a low vehicle traffic density, the value of K_{pq} is very large since the LoS component can bear a significant amount of power. Furthermore, we assume that the values of the energy parameters η_{SB_1} and η_{SB_2} related to single-bounced rays of the two-ring model are very small or close to zero. This is due to the fact that the received scattered power is mainly from waves reflected by the buildings located on the roadsides. These waves form double-bounced rings of the two-ring model and single-bounced rays of the elliptical-ring model, in which single-bounced rays of the elliptical-ring model bear more energy than double-bounced rays of the two-ring model due to the high dependency between the AoAs and AoDs, i.e., $\eta_{SB_3} > \eta_{DB} \gg \max\{\eta_{SB_1}, \eta_{SB_2}\}$. When the vehicle traffic density is high, the value of K_{pq} is smaller than that in the low vehicle traffic density scenario. In this case, double-bounced rays of the two-ring model bear more energy than single-bounced rays of the two-ring model and elliptical-ring model due to the independency between the AoAs and AoDs, i.e, $\eta_{DB} \gg \max\{\eta_{SB_1}, \eta_{SB_2}, \eta_{SB_3}\}$. To the best of the authors' knowledge, all the existing MIMO M2M channel models [4], [5] have no ability to model pico-cell propagation environments considering different vehicle traffic densities.

Distances ϵ_{pq}, ϵ_{pn_i}, ϵ_{n_iq}, and $\epsilon_{n_1n_2}$ in (1)–(4) can be expressed as functions of the relevant angles, e.g., $\phi_{R_q}^{LoS}$, $\phi_T^{(n_i)}$, and $\phi_R^{(n_i)}$, for the aforementioned different scenarios. From Fig. 1, assuming $D \gg \max\{\delta_T, \delta_R\}$ and invoking the laws of sines and cosines, these distances are

1) For the LoS component,

$$\epsilon_{pq} \approx \epsilon - k_q\delta_R \cos\left(\phi_{R_q}^{LoS} - \beta_R\right) \quad (5)$$

$$\epsilon \approx D - k_p\delta_T \cos\beta_T \quad (6)$$

where for the macro- and micro-cell scenarios $\phi_{R_q}^{LoS} \approx \pi$ ($D \gg \max\{R_T, R_R\}$), while for the pico-cell scenario $\phi_{R_q}^{LoS} \approx \pi - k_p\delta_T \sin\beta_T / D$ ($D \gg \max\{R_T, R_R\}$ not fulfilled) with $k_p = (M_T - 2p + 1)/2$ and $k_q = (M_R - 2q + 1)/2$.

2) For the single-bounced component of the two-ring model,

$$\epsilon_{pn_1} \approx R_T - k_p\delta_T \cos\left(\phi_T^{(n_1)} - \beta_T\right) \quad (7)$$

$$\epsilon_{n_1q} \approx \xi_{n_1} - k_q\delta_R \cos\left(\phi_R^{(n_1)} - \beta_R\right) \quad (8)$$

$$\epsilon_{pn_2} \approx \xi_{n_2} - k_p\delta_T \cos\left(\phi_T^{(n_2)} - \beta_T\right) \quad (9)$$

$$\epsilon_{n_2q} \approx R_R - k_q\delta_R \cos\left(\phi_R^{(n_2)} - \beta_R\right) \quad (10)$$

where for the macro- and micro-cell scenarios $\xi_{n_1} \approx D - R_T \cos\phi_T^{(n_1)}$, $\phi_R^{(n_1)} \approx \pi - \Delta_T \sin\phi_T^{(n_1)}$, $\xi_{n_2} \approx D + R_R \cos\phi_R^{(n_2)}$, and $\phi_T^{(n_2)} \approx \Delta_R \sin\phi_R^{(n_2)}$ ($D \gg \max\{R_T, R_R\}$) with $\Delta_T \approx R_T/D$ and $\Delta_R \approx R_R/D$, while for the pico-cell scenario the condition $D \gg \max\{R_T, R_R\}$ is not fulfilled anymore. This enforces us to find a new general relationship between the AoA and AoD for a geometrical-based model with single-bounced rays. From Fig. 1, using the laws of sines and cosines to the triangles $O_TT_pO_R$ and $O_TT_pO_R$, we have

$$\xi_{n_1} = \left(D^2 + R_T^2 - 2DR_T\cos\phi_T^{(n_1)}\right)^{1/2} \quad (11)$$

$$\sin\phi_R^{(n_1)} \approx \left(k_q\delta_R\cos\beta_R\Gamma_{TA} - d_p\Gamma_{TB}\right)/2k_q\delta_R d_p\xi_{n_1}\Gamma_{TC} \quad (12)$$

$$\cos\phi_R^{(n_1)} \approx \frac{k_q\delta_R\sin\beta_R\Gamma_{TA} + \left(d_pk_p\delta_T\sin\beta_T\Gamma_{TB}\right)/D}{2k_q\delta_R d_p\xi_{n_1}\Gamma_{TC}} \quad (13)$$

$$\xi_{n_2} = \left(D^2 + R_R^2 + 2DR_R\cos\phi_R^{(n_2)}\right)^{1/2} \quad (14)$$

$$\sin\phi_T^{(n_2)} \approx \left(k_p\delta_T\cos\beta_T\Gamma_{RA} - d_q\Gamma_{RB}\right)/2k_p\delta_T d_q\xi_{n_2}\Gamma_{RC} \quad (15)$$

$$\cos\phi_T^{(n_2)} \approx \frac{\left(d_qk_q\delta_R\sin\beta_R\Gamma_{RB}\right)/D - k_p\delta_T\sin\beta_T\Gamma_{RA}}{2k_p\delta_T d_q\xi_{n_2}\Gamma_{RC}}. \quad (16)$$

Here, parameters Γ_{TA}, Γ_{TB}, Γ_{TC}, Γ_{RA}, Γ_{RB}, and Γ_{RC} are $\Gamma_{TA} = \xi_{n_1}^2 + k_q^2\delta_R^2 - R_T^2 - d_q^2 + 2R_Td_q\cos\left(\phi_T^{(n_1)} - \theta_q\right)$, $\Gamma_{TB} = R_T^2 + k_p^2\delta_T^2 - \xi_{n_1}^2 - d_p^2 - 2k_p\delta_TR_T\cos\left(\phi_T^{(n_1)} - \beta_T\right)$, $\Gamma_{TC} = \left(k_p\delta_T\sin\beta_T\cos\beta_R\right)/D + \sin\beta_R$, $\Gamma_{RA} = \xi_{n_2}^2 + d_q^2 - R_R^2 - k_q^2\delta_R^2 + 2k_q\delta_RR_R\cos\left(\phi_R^{(n_2)} - \beta_R\right)$, $\Gamma_{RB} = \xi_{n_2}^2 + k_p^2\delta_T^2 - R_R^2 - d_p^2 - 2d_pR_R\cos\left(\phi_R^{(n_2)} + \theta_p\right)$, and $\Gamma_{RC} = \left(k_q\delta_R\sin\beta_R\cos\beta_T\right)/D - \sin\beta_T$, respectively, with $\cos\theta_p = \cos\theta_q \approx 1$, $\sin\theta_p \approx \left(k_p\delta_T\sin\beta_T\right)/D$, $\sin\theta_q \approx \left(k_q\delta_R\sin\beta_R\right)/D$, $d_p \approx D - k_p\delta_T\cos\beta_T$, and $d_q \approx D + k_q\delta_R\cos\beta_R$.

3) For the single-bounced component of the elliptical-ring model,

$$\epsilon_{pn_3} \approx \xi_T^{(n_3)} - k_p\delta_T\cos\left(\phi_T^{(n_3)} - \beta_T\right) \quad (17)$$

$$\epsilon_{n_3q} \approx \xi_R^{(n_3)} - k_q\delta_R\cos\left(\phi_R^{(n_3)} - \beta_R\right) \quad (18)$$

$$\xi_T^{(n_3)} = \left(a^2 + D^2/4 + aD\cos\phi_R^{(n_3)}\right)/\left(a + D\cos\phi_R^{(n_3)}/2\right) \quad (19)$$

$$\xi_R^{(n_3)} = b^2/\left(a + D\cos\phi_R^{(n_3)}/2\right) \quad (20)$$

$$\xi_T^{(n_3)} + \xi_R^{(n_3)} = 2a \quad (21)$$

following the similar reasoning as (12) and (13), we have

$$\sin\phi_T^{(n_3)} \approx \frac{k_p\delta_T\cos\beta_T\Gamma_{RA_E} - d_q\Gamma_{RB_E}}{2k_p\delta_T d_q\xi_T^{(n_3)}\Gamma_{RC}} \quad (22)$$

$$\cos\phi_T^{(n_3)} \approx \frac{\left(d_qk_q\delta_R\sin\beta_R\Gamma_{RB_E}\right)/D - k_p\delta_T\sin\beta_T\Gamma_{RA_E}}{2k_p\delta_T d_q\xi_T^{(n_3)}\Gamma_{RC}} \quad (23)$$

where parameters Γ_{RA_E} and Γ_{RB_E} are $\Gamma_{RA_E} = {\xi_T^{(n_3)}}^2 + d_q^2 - {\xi_R^{(n_3)}}^2 - k_q^2\delta_R^2 + 2k_q\delta_R\xi_R^{(n_3)}\cos\left(\phi_R^{(n_3)} - \beta_R\right)$ and $\Gamma_{RB_E} = {\xi_T^{(n_3)}}^2 + k_p^2\delta_T^2 - {\xi_R^{(n_3)}}^2 - d_p^2 - 2d_p\xi_R^{(n_3)}\cos\left(\phi_R^{(n_3)} + \theta_p\right)$, respectively, and b denotes the semi-minor axis of the ellipse.

4) For the double-bounced component of the two-ring model,

$$\epsilon_{pn_1} \approx R_T - k_p\delta_T\cos\left(\phi_T^{(n_1)} - \beta_T\right) \quad (24)$$

$$\epsilon_{n_2q} \approx R_R - k_q\delta_R\cos\left(\phi_R^{(n_2)} - \beta_R\right) \quad (25)$$

where for the macro- and micro-cell scenarios $\epsilon_{n_1n_2} \approx D$ ($D \gg \max\{R_T, R_R\}$), while for the pico-cell scenario $\epsilon_{n_1n_2} \approx D - R_T\cos\phi_T^{(n_1)} + R_R\cos\phi_R^{(n_2)}$ ($D \gg \max\{R_T, R_R\}$ not fulfilled).

In this paper, to characterize the AoD $\phi_T^{(n_i)}$ and AoA $\phi_R^{(n_i)}$, we use the von Mises probability density function (PDF) [8] defined as $f(\phi) \triangleq \exp[k\cos(\phi-\mu)]/2\pi I_0(k)$, where $\phi \in [-\pi,\pi)$, $I_0(\cdot)$ is the zeroth-order modified Bessel function of the first kind, $\mu \in [-\pi,\pi)$ accounts for the mean value of the angle ϕ, and k ($k \geq 0$) is a real-valued parameter that controls the angle spread of the angle ϕ.

III. ST CF AND SD PSD

In this section, based on the proposed channel model in (1)–(4), we will derive the ST CF and the corresponding SD PSD for a 2-D non-isotropic scattering environment.

A. The ST CF

The normalized ST CF between any two complex impulse responses $h_{pq}(t)$ and $h_{p'q'}(t)$ is defined as

$$\rho_{h_{pq}h_{p'q'}}(\tau) = \frac{\mathbf{E}\left[h_{pq}(t)\,h^*_{p'q'}(t+\tau)\right]}{\sqrt{\mathbf{E}\left[|h_{pq}(t)|^2\right]\mathbf{E}\left[|h_{p'q'}(t)|^2\right]}} \tag{26}$$

where $(\cdot)^*$ denotes the complex conjugate operation, $\mathbf{E}[\cdot]$ is the statistical expectation operator, $p,p' \in \{1,2,...,M_T\}$, and $q,q' \in \{1,2,...,M_R\}$. It should be observed that (26) is a function of time separation τ and antenna element spacings δ_T and δ_R.

Using trigonometric transformations, the equality $\int_{-\pi}^{\pi}\exp(a \times \sin c + b\cos c)dc = 2\pi I_0\left(\sqrt{a^2+b^2}\right)$ [9], and the results in [6] without considering frequency correlations [**?**], the ST CF of the LoS, single-, and double-bounced components for different scenarios can be obtained as

1) In the case of the LoS component,

$$\rho_{h_{pq}^{LoS}h_{p'q'}^{LoS}}(\tau) = \sqrt{K_{pq}K_{p'q'}}\,e^{j2\pi G - j2\pi\tau H} \tag{27}$$

where for the macro- and micro-cell scenarios $G=P\cos\beta_T - Q\cos\beta_R$ and $H=f_{T_{max}}\cos\gamma_T - f_{R_{max}}\cos\gamma_R$, while for the pico-cell scenario $G = P\cos\beta_T - Q\cos\beta_R + \sin\beta_T\sin\beta_R\left(P\left(M_R+1\right)\delta_R + Q\left(M_T+1\right)\delta_T - 2U\right)/(2D)$ and $H=f_{T_{max}}\left(\cos\gamma_T + k_{p'}\delta_T\sin\beta_T\sin\gamma_T/D\right) + f_{R_{max}}\left(k_{p'}\delta_T \times \sin\beta_T\sin\gamma_R - \cos\gamma_R/D\right)$, with $P=(p'-p)\,\delta_T/\lambda$, $Q=(q'-q)\,\delta_R/\lambda$, $U=(p'q'-pq)\,\delta_T\delta_R/\lambda$, $k_{p'}=\left(M_T-2p'+1\right)/2$, and $k_{q'}=\left(M_R-2q'+1\right)/2$.

2) In the case of the single-bounced component of the two-ring model, for macro- and micro-cell scenarios

$$\rho_{h_{pq}^{SB_i}h_{p'q'}^{SB_i}}(\tau) = \eta_{SB_i}e^{jC_T^{SB_i}}\frac{I_0\left[\sqrt{\left(A_{T(R)}^{SB_i}\right)^2+\left(B_{T(R)}^{SB_i}\right)^2}\right]}{I_0\left(k_{T(R)}^{SB_i}\right)} \tag{28}$$

where parameters $A_T^{SB_1}$, $B_T^{SB_1}$, $C_T^{SB_1}$, $A_R^{SB_2}$, $B_R^{SB_2}$, and $C_R^{SB_2}$ are $A_T^{SB_1} = k_T^{SB_1}\cos\mu_T^{SB_1} - j2\pi\left(\tau f_{T_{max}}\cos\gamma_T + P\cos\beta_T\right)$, $B_T^{SB_1} = k_T^{SB_1}\sin\mu_T^{SB_1} - j2\pi\left(\tau f_{T_{max}}\sin\gamma_T - \tau f_{R_{max}}\Delta_T\sin\gamma_R + P\sin\beta_T + Q\Delta_T\sin\beta_R\right)$, $C_T^{SB_1}=2\pi\left(\tau f_{R_{max}}\cos\gamma_R - Q\cos\beta_R\right)$, $A_R^{SB_2}=k_R^{SB_2}\cos\mu_R^{SB_2} - j2\pi\left(\tau f_{R_{max}}\cos\gamma_R + Q\cos\beta_R\right)$, $B_R^{SB_2} = k_R^{SB_2}\sin\mu_R^{SB_2} - j2\pi\left(\tau f_{R_{max}}\sin\gamma_R - \tau f_{T_{max}}\Delta_R\sin\gamma_T + Q\sin\beta_R + P\Delta_R\sin\beta_T\right)$, and $C_R^{SB_2} = 2\pi\left(\tau f_{T_{max}}\cos\gamma_T + P\cos\beta_T\right)$, respectively,with $\mu_T^{SB_1}$ $\left(\mu_R^{SB_2}\right)$ denoting the mean value of the AoD $\phi_T^{(n_1)}$ (AoA $\phi_R^{(n_2)}$) and $k_T^{SB_1}$ $\left(k_R^{SB_2}\right)$ controls the angle spread of the AoD $\phi_T^{(n_1)}$ (AoA $\phi_R^{(n_2)}$). For pico-cell scenarios, the ST CF of single-bouced components of the two-ring model is given as

$$\rho_{h_{pq}^{SB_i}h_{p'q'}^{SB_i}}(\tau) = \frac{\eta_{SB_i}}{2\pi I_0\left(k_{T(R)}^{SB_i}\right)}\int_{-\pi}^{\pi}e^{J_i + j2\pi(T_i - \tau V_i)}d\phi_{T(R)}^{SB_i} \tag{29}$$

where $J_1=k_T^{SB_1}\cos\left(\phi_T^{SB_1}-\mu_T^{SB_1}\right)$, $T_1=P\cos\left(\phi_T^{SB_1}-\beta_T\right) + Q\cos\left(\phi_R^{SB_1}-\beta_R\right)$, $V_1 = f_{T_{max}}\cos\left(\phi_T^{SB_1}-\gamma_T\right) + f_{R_{max}}\cos\left(\phi_R^{SB_1}-\gamma_R\right)$, $J_2 = k_R^{SB_2}\cos\left(\phi_R^{SB_2}-\mu_R^{SB_2}\right)$, $T_2 = P\cos\left(\phi_T^{SB_2}-\beta_T\right) + Q\cos\left(\phi_R^{SB_2}-\beta_R\right)$, and $V_2 = f_{T_{max}}\cos\left(\phi_T^{SB_2}-\gamma_T\right) + f_{R_{max}}\cos\left(\phi_R^{SB_2}-\gamma_R\right)$, with $\phi_T^{SB_1}$, $\phi_R^{SB_1}$, $\phi_T^{SB_2}$, and $\phi_R^{SB_2}$ are the continuous notations of $\phi_T^{(n_1)}$, $\phi_R^{(n_1)}$, $\phi_T^{(n_2)}$, and $\phi_R^{(n_2)}$, respectively, since we assume that the number of local scatterers in the proposed reference model in Section II tends to infinite.

3) In terms of the single-bounced component of the elliptical-ring model,

$$\rho_{h_{pq}^{SB_3}h_{p'q'}^{SB_3}}(\tau) = \frac{\eta_{SB_3}}{2\pi I_0\left(k_R^{SB_3}\right)}\int_{-\pi}^{\pi}e^{J_3 + j2\pi(T_3 - \tau V_3)}d\phi_R^{SB_3} \tag{30}$$

where $J_3=k_R^{SB_3}\cos\left(\phi_R^{SB_3}-\mu_R^{SB_3}\right)$, $T_3=P\cos\left(\phi_T^{SB_3}-\beta_T\right) + Q\cos\left(\phi_R^{SB_3}-\beta_R\right)$, and $V_3 = f_{T_{max}}\cos\left(\phi_T^{SB_3}-\gamma_T\right) + f_{R_{max}}\cos\left(\phi_R^{SB_3}-\gamma_R\right)$, with $\phi_T^{SB_3}$ and $\phi_R^{SB_3}$ are the continuous notations of $\phi_T^{(n_3)}$ and $\phi_R^{(n_3)}$, respectively. The parameter $\mu_R^{SB_3}$ denotes the mean value of the AoA $\phi_R^{SB_3}$ and $k_R^{SB_3}$ controls the angle spread of the AoA $\phi_R^{SB_3}$.

4) In terms of the double-bounced component of the two-ring model,

$$\rho_{h_{pq}^{DB}h_{p'q'}^{DB}}(\tau) = \eta_{DB} \times \frac{I_0\left\{\sqrt{\left(A_T^{DB}\right)^2+\left(B_T^{DB}\right)^2}\right\}I_0\left\{\sqrt{\left(A_R^{DB}\right)^2+\left(B_R^{DB}\right)^2}\right\}}{I_0\left(k_T^{DB}\right)I_0\left(k_R^{DB}\right)} \tag{31}$$

where $A_T^{DB} = k_T^{DB}\cos\mu_T^{DB} - j2\pi\left(\tau f_{T_{max}}\cos\gamma_T + P\cos\beta_T\right)$, $B_T^{DB}=k_T^{DB}\sin\mu_T^{DB} - j2\pi\left(\tau f_{T_{max}}\sin\gamma_T + P\sin\beta_T\right)$, $A_R^{DB} = k_R^{DB}\cos\mu_R^{DB} - j2\pi\left(\tau f_{R_{max}}\cos\gamma_R + Q\cos\beta_R\right)$, and $B_R^{DB} = k_R^{DB}\sin\mu_R^{DB} - j2\pi\left(\tau f_{R_{max}}sin\gamma_R + Q\sin\beta_R\right)$.Finally, the normalized ST CF between two time-variant complex impulse responses $h_{pq}(t)$ and $h_{p'q'}^{(\dagger)}(t)$ becomes a summation of the ST CFs in (27)–(31).

B. The SD PSD

Applying the Fourier transformation in terms of time to the ST CF in (26), the corresponding SD PSD can be obtained as

$$F\left\{\rho_{h_{pq}h_{p'q'}}(\tau)\right\} = \int_{-\infty}^{\infty}\rho_{h_{pq}h_{p'q'}}(\tau)\,e^{-j2\pi f_D\tau}d\tau \tag{32}$$

where f_D is the Doppler frequency. The integral in (32) must be evaluated numerically in the case of the two-ring model with single-bounced rays for pico-cell scenarios and the elliptical-ring model for all scenarios. While for other cases, by using the equality $\int_0^\infty I_0\left(j\alpha\sqrt{x^2+y^2}\right)\cos(\beta x)\,dx = \cos\left(y\sqrt{\alpha^2-\beta^2}\right)/\sqrt{\alpha^2-\beta^2}$ [9] and the results in [6], we can further get closed-form solutions.

1) In the case of the LoS component,

$$F\left\{\rho_{h_{pq}^{LoS}h_{p'q'}^{LoS}}(\tau)\right\} = \sqrt{K_{pq}K_{p'q'}}e^{j2\pi G}\delta(f_D+H) \quad (33)$$

where $\delta(\cdot)$ denotes the Dirac delta function.

2) In terms of the single-bounced component of two-ring model,

$$F\left\{\rho_{h_{pq}^{SB_i}h_{p'q'}^{SB_i}}(\tau)\right\} = \frac{\eta_{SB_i}2e^{jU_{T(R)}^{SB_i}+j2\pi O_{T(R)}^{SB_i}\frac{D_{T(R)}^{SB_i}}{W_{T(R)}^{SB_i}}}}{I_0\left(k_{T(R)}^{SB_i}\right)} \times \frac{\cos\left[\frac{E_{T(R)}^{SB_i}}{W_{T(R)}^{SB_i}}\sqrt{W_{T(R)}^{SB_i}-4\pi^2\left(O_{T(R)}^{SB_i}\right)^2}\right]}{\sqrt{W_{T(R)}^{SB_i}-4\pi^2\left(O_{T(R)}^{SB_i}\right)^2}} \quad (34)$$

where $U_T^{SB_1}=-2\pi Q\cos\beta_R$, $U_T^{SB_2}=2\pi P\cos\beta_T$, $W_T^{SB_1}=4\pi^2\left(f_{T_{max}}^2+f_{R_{max}}^2\Delta_T^2\sin\gamma_R^2+2f_{T_{max}}f_{R_{max}}\Delta_T\sin\gamma_T\sin\gamma_R\right)$, $W_R^{SB_2}=4\pi^2\left(f_{R_{max}}^2+f_{T_{max}}^2\Delta_R^2\sin\gamma_T^2+2f_{R_{max}}f_{T_{max}}\Delta_R\sin\gamma_R\times\sin\gamma_T\right)$, $D_T^{SB_1}=j2\pi k_T^{SB_1}\left[f_{T_{max}}\cos\left(\gamma_T-\mu_T^{SB_1}\right)+f_{R_{max}}\Delta_T\times\sin\gamma_R\sin\mu_T^{SB_1}\right]-4\pi^2\left[Pf_{T_{max}}\cos(\beta_T-\gamma_T)-Q\Delta_Tf_{T_{max}}\times\sin\beta_R\sin\gamma_T-P\Delta_Tf_{R_{max}}\sin\beta_T\sin\gamma_R-Q\Delta_T^2f_{R_{max}}\sin\beta_R\times\sin\gamma_R\right]$, $D_R^{SB_2}=j2\pi k_R^{SB_2}\left[f_{R_{max}}\cos\left(\gamma_R-\mu_R^{SB_2}\right)+f_{T_{max}}\Delta_R\times\sin\gamma_T\sin\mu_R^{SB_2}\right]-4\pi^2\left[Qf_{R_{max}}\cos(\beta_R-\gamma_R)-P\Delta_Rf_{R_{max}}\times\sin\beta_T\sin\gamma_R-Q\Delta_Rf_{T_{max}}\sin\beta_R\sin\gamma_T-P\Delta_T^2f_{T_{max}}\sin\beta_T\times\sin\gamma_T\right]$, $E_T^{SB_1}=j2\pi k_T^{SB_1}\left[f_{T_{max}}\sin\left(\gamma_T-\mu_T^{SB_1}\right)+f_{R_{max}}\Delta_T\times\sin\gamma_R\cos\mu_T^{SB_1}\right]-4\pi^2\left[Pf_{T_{max}}\sin(\beta_T-\gamma_T)-Q\Delta_Tf_{T_{max}}\times\sin\beta_R\cos\gamma_T-P\Delta_Tf_{R_{max}}\cos\beta_T\sin\gamma_R\right]$, $E_R^{SB_2}=j2\pi k_R^{SB_2}\left[f_{R_{max}}\sin\left(\gamma_R-\mu_R^{SB_2}\right)+f_{T_{max}}\Delta_R\sin\gamma_T\cos\mu_R^{SB_2}\right]-4\pi^2\left[Qf_{R_{max}}\sin(\beta_R-\gamma_R)-P\Delta_Rf_{R_{max}}\sin\beta_T\cos\gamma_R-Q\Delta_Rf_{T_{max}}\times\cos\beta_R\sin\gamma_T\right]$, $O_T^{SB_1}=f-f_{R_{max}}\cos\gamma_R$, $O_R^{SB_2}=f+f_{T_{max}}\cos\gamma_T$, $|f_D-f_{R_{max}}\cos\gamma_R|\le\sqrt{W_T^{SB_1}}/(2\pi)$, and $|f_D+f_{T_{max}}\cos\gamma_T|\le\sqrt{W_R^{SB_2}}/(2\pi)$.

3) In terms of the double-bounced component of two-ring model,

$$F\left\{\rho_{h_{pq}^{DB}h_{p'q'}^{DB}}(\tau)\right\} = \frac{\eta_{DB}e^{jC^{DB}}}{I_0\left(k_T^{DB}\right)I_0\left(k_R^{DB}\right)} \times 2e^{j2\pi f\frac{D_T^{DB}}{W_T^{DB}}}\frac{cos\left(\frac{E_T^{DB}}{W_T^{DB}}\sqrt{W_T^{DB}-4\pi^2f^2}\right)}{\sqrt{W_T^{DB}-4\pi^2f^2}} \odot 2e^{j2\pi f\frac{D_R^{DB}}{W_R^{DB}}}\frac{cos\left(\frac{E_R^{DB}}{W_R^{DB}}\sqrt{W_R^{DB}-4\pi^2f^2}\right)}{\sqrt{(W_R^{DB}-4\pi^2f^2}} \quad (35)$$

where $\odot$ denotes the convolution, $D_T^{DB}=-4\pi^2Pf_{T_{max}}\cos(\beta_T-\gamma_T)+j2\pi k_T^{DB}f_{T_{max}}cos\left(\gamma_T-\mu_T^{DB}\right)$, $E_T^{DB}=4\pi^2Pf_{T_{max}}\sin(\beta_T-\gamma_T)+j2\pi k_T^{DB}f_{T_{max}}\sin\left(\gamma_T-\mu_T^{DB}\right)$, $D_R^{DB}=-4\pi^2Qf_{R_{max}}\cos(\beta_R-\gamma_R)+j2\pi k_R^{DB}f_{R_{max}}\cos\left(\gamma_R-\mu_R^{DB}\right)$, $E_R^{DB}=4\pi^2Qf_{R_{max}}\sin(\beta_R-\gamma_R)+j2\pi k_R^{DB}f_{R_{max}}\sin\left(\gamma_R-\mu_R^{DB}\right)$, $W_T^{DB}=4\pi^2f_{T_{max}}^2$, $W_R^{DB}=4\pi^2f_{R_{max}}^2$, and $|f|\le\left(\sqrt{W_T^{DB}}+\sqrt{W_R^{DB}}\right)/(2\pi)=f_{T_{max}}+f_{R_{max}}$.

IV. Numerical Results and Analyses

In this section, we first present the numerical results of the Doppler PSD for elliptical-ring model with single-bounced rays and then show some numerical evaluations of the proposed theoretical model. The following parameters are used for our numerical analysis: $f_c = 5.9$ GHz, $f_{T_{max}} = f_{R_{max}} = 570$ Hz, $D = 350$ m, $a = 250$ m, and $R_T = R_R = 30$ m.

From Fig. 2, it is clear that the shape of the Doppler PSD for the elliptical-ring model with single-bounced rays is similar to the U-shape PSD in F2M channels. Considering observations in [6], we can further get another interesting conclusion that no matter what the propagation environment is, for M2M channels in isotropic scattering environments, the single-bounced rays cause the resulting Doppler PSDs to look like the U-shape, while the double-bounced rays will result in a "rounded"-shape Doppler PSD. Figs. 3 and 4 show the SD PSDs for a MIMO M2M Ricean fading channel with different antenna element spacings in an outdoor pico-cell scenario, where the Tx and Rx are moving in the same direction on an expressway, with a low and a high vehicle traffic density, respectively. Considering the real environment behind the measurement result of Fig. 6 in [7], where large stationary objects are available along this expressway, and following the way to specify the Ricean factor and energy-related parameters regarding different scenarios given in Section II, in Fig. 3 we assume $K = 2$, $\eta_{DB} = 0.01$, $\eta_{SB_1} = 0.299$, $\eta_{SB_2} = 0.091$, and $\eta_{SB_3} = 0.6$. Similarly, Fig. 4 assumes $K = 0.5$, $\eta_{DB} = 0.7$, $\eta_{SB_1} = 0.19$, $\eta_{SB_2} = 0.01$, and $\eta_{SB_3} = 0.1$ for the real environment where the main received power is reflected by cars around the Tx or Rx. The measurement result of Fig. 9 in [7] was obtained from this type of scenario. Finally, comparing our theoretical Doppler PSDs obtained for $\delta_T = \delta_R = 0$ in Figs. 3 and 4 with measured Doppler PSDs of Figs. 6 and 9 in [7], respectively, we can obtain the close agreement confirming the usefulness of the proposed model.

V. Conclusions

In this paper, we have proposed a generic and adaptive geometrical-based stochastic model for MIMO M2M Ricean fading channels. Considering the impact of separation distance and energy specified parameters, the proposed model is adaptable to a wide variety of M2M propagation environments. From this model, the ST CF and the corresponding SD PS for 2D non-isotropic scattering environments are derived. Based on the obtained Doppler PSD for the elliptical-ring model with single-bounced rays and observations in [6], we conclude that no matter what the propagation environment is, single-bounced

rays cause the Doppler PSD look like the traditional U-shape, while double-bounced rays result in a "rounded"-shape Doppler PSD for M2M channels in non-isotropic scattering environments. Finally, the resulting theoretical SD PSDs match very well measured PSDs in [7].

REFERENCES

[1] A. S. Akki and F. Haber, "A statistical model for mobile-to-mobile land communication channel," *IEEE Trans. Veh. Technol.*, vol. 35, no. 1, pp. 2–10, Feb. 1986.

[2] A. S. Akki, "Statistical properties of mobile-to-mobile land communication channels," *IEEE Trans. Veh. Technol.*, vol. 43, no. 4, pp. 826–831, Nov. 1994.

[3] J. M. G. Linnartz and R. F. Fiesta. (1996) Evaluation of radio links and networks. [Online]. Available: http://www.path.berkeley.edu/PATH/Publications/PDF/PRR/96/PRR-96-16.pdf.

[4] M. Pätzold, B. O. Hogstad, N. Youssef, and D. Kim, "A MIMO mobile-to-mobile channel model: Part I–the reference model," *Proc. IEEE PIMRC'05*, Berlin, Germany, Sept. 2005, pp. 573–578.

[5] A. G. Zajić and G. L. Stüber, "Space-time correlated mobile-to-mobile channels: modelling and simulation," *IEEE Trans. Veh. Technol.*, vol. 57, no. 2, pp. 715–726, Mar. 2008.

[6] X. Cheng, C.-X. Wang, D. I. Laurenson, H. H. Chen, and A. V. Vasilakos, "Space-time-frequency characterization of non-isotropic MIMO mobile-to-mobile multicarrier Ricean fading channels," *IEEE IWCMC'08*, Chania Crete Island, Greece, Aug. 2008, accepted for publication.

[7] G. Acosta, K. Tokuda, and M. A. Ingram, "Doubly selective vehicle traffic-to-vehicle traffic channel measurements and modeling at 5.9 GHz," *Proc. IEEE WPMC'06*, San Diego, CA, USA, Sep. 2006, pp. 1–6.

[8] A. Abdi, J. A. Barger, and M. Kaveh, "A parametric model for the distribution of the angle of arrival and the associated correlation function and power spectrum at the mobile station," *IEEE Trans. Veh. Technol.*, vol. 51, no. 3, pp. 425–434, May 2002.

[9] I. S. Gradshteyn, and I. M. Ryzhik, *Table of Integrals, Series, and Products*. 5th ed, A. Jeffrey, Ed. San Diego, CA: Academic, 1994.

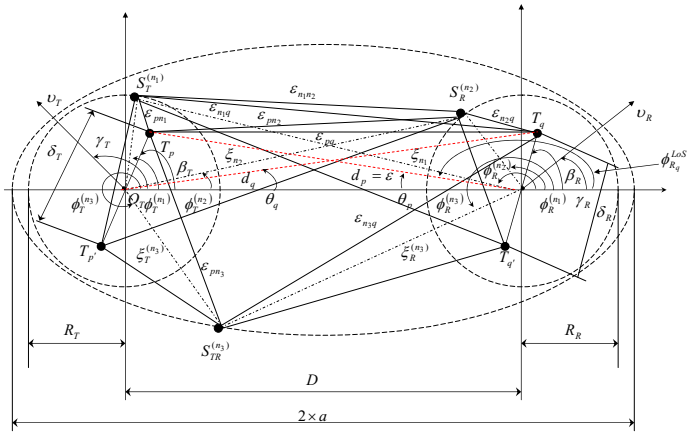

Fig. 1. The proposed model with the LoS, Single- and double-bounced components for a MIMO M2M channel with $M_T = M_R = 2$ antenna elements.

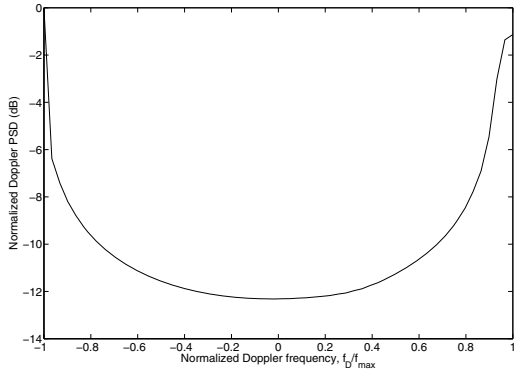

Fig. 2. Normalized space-Doppler PSD of the elliptical-ring model with single-bounced rays ($f = 5.9$ GHz, $f_{T_{max}} = f_{R_{max}} = 570$ Hz, $\gamma_T = \gamma_R = 0$, $\mu_T = 0$, $\mu_R = \pi$, $k_T = k_R = \delta_T = \delta_R = 0$, and $M_T = M_R = 2$).

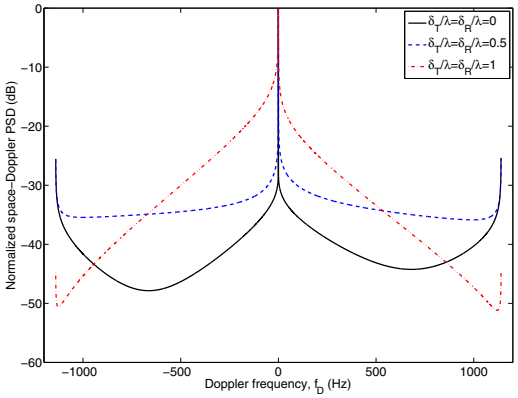

Fig. 3. Normalized space-Doppler PSDs for the outdoor pico-cell scenario having a low vehicle traffic density with different antenna element spacings ($f = 5.9$ GHz, $f_{T_{max}} = f_{R_{max}} = 570$ Hz, $K = 2$, $\gamma_T = \gamma_R = 0$, $\mu_T = 0$, $\mu_R = \pi$, $k_T = 3$, $k_R = 2$, and $M_T = M_R = 2$).

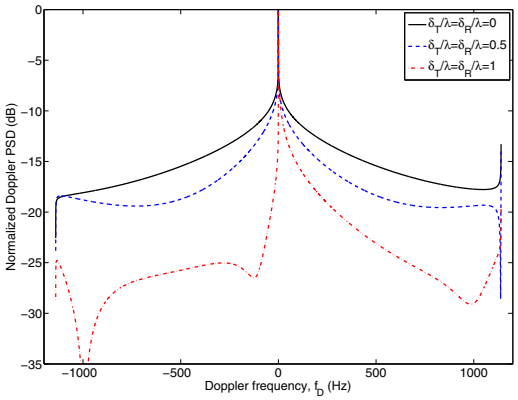

Fig. 4. Normalized space-Doppler PSDs for the outdoor pico-cell scenario having a high vehicle traffic density with different antenna element spacings ($f = 5.9$ GHz, $f_{T_{max}} = f_{R_{max}} = 570$ Hz, $K = 0.5$, $\gamma_T = \gamma_R = 0$, $\mu_T = 0$, $\mu_R = \pi$, $k_T = k_R = 1$, and $M_T = M_R = 2$).